Journal of Modern Optics
Vol. 00, No. 00, 00 Month 200x, 1–9

Streaking analysis of strong-field ionization

Manfred Lein

Institut für Theoretische Physik
and Centre for Quantum Engineering and Space-Time Research (QUEST),
Leibniz Universität Hannover, Appelstraße 2, 30167 Hannover, Germany

(*dated December 17, 2010*)

Motivated by recent experimental progress in precision investigation of strong-field ionization by angular streaking [Eckle *et al.*, Science **322** 1525 (2008)], we employ streaking by a linearly polarized half-cycle pulse as a theoretical tool to analyze the strong-field ionization of atoms. For moderate field strengths, the electron momentum distribution is consistent with the interpretation that ionization occurs most probably at the peak of the field followed by classical electron motion under the combined force of the laser field and the atomic potential. At high field strengths, the momentum distributions together with the classical model indicate that ionization occurs preferentially before the peak of the field. Surprisingly, the momentum at the peak of the distribution scales almost linearly with the intensity of the half-cycle pulse.

Keywords: strong-field ionization; streaking; Coulomb correction; Stark shift

1. Introduction

The response of atoms and molecules to strong laser pulses at intensities above $10^{14}\,\mathrm{W/cm^2}$ has become the main avenue to study matter on the subfemtosecond time scale. This includes not only the generation of attosecond pulses through high-order harmonic generation [1], but also ultrafast imaging using laser-driven electron wave packets [2–5]. The development of this field is strongly based on the semiclassical interpretation of the ionization dynamics: after emergence of an electron in the continuum, its further time evolution may be approximately described by the classical equation of motion. Although the details of the ionization step itself and the recombination in high-order harmonic generation must be treated quantum mechanically [6–8], classical continuum dynamics explains successfully the cutoffs in the photon and electron spectra [9, 10] as well as the attosecond chirp of high-harmonic radiation [1, 11]. In a quasistatic picture for low-frequency laser fields, the ionization rate is determined by the instantaneous electric field that is applied to the system. The maximum instantaneous ionization rate is thus expected to be caused by the maximum absolute value of the electric field of the laser pulse. This is predicted also in the nonadiabatic tunnel ionization theory [6].

Recently, angular streaking was used as an experimental tool to carry out a precision investigation of laser-induced ionization [12, 13]. The method uses elliptically polarized few-cycle laser pulses to ionize rare-gas atoms. From the detected emission angle of an outgoing electron or ion, one can deduce the time at which the electron has emerged from the barrier formed by the atomic potential and the laser field. To this end, one assumes that the electron emerges via a tunnelling process and continues on a classical trajectory under the force exerted by the laser field and the parent ion, starting with zero velocity at the exit of the tunnel. The peak in the momentum distribution identifies the most probable electron trajectory in ionization. Angular streaking has been interpreted such that the most probable trajectory is caused by the maximum instantaneous value of the electric field. The experimental results for the helium atom indicate

ISSN: 0950-0340 print/ISSN 1362-3044 online

DOI: 10.1080/0950034YYxxxxxxxx
http://www.informaworld.com

an upper limit of 34 attoseconds for the tunnelling delay time, i.e. the difference between the emergence time at the tunnel exit and the peak of the electric field. This tunnelling delay time is extremely short as compared to the Keldysh tunnelling time or Büttiker-Landauer traversal time [14, 15], which is evaluated to be about 500 attoseconds for the experimental situation (intensity $\sim 0.3\,\mathrm{PW/cm^2}$, wavelength 725 nm). Hence, tunnelling is thought to be practically "instantaneous" on the scale of the laser optical cycle of ~ 2.4 fs.

Elliptically polarized laser pulses give rise to momentum distributions peaked at nonzero momentum. The ionization times within one laser cycle are mapped on emission angles in the full 360^o range. This makes elliptical polarization, unlike linear polarization, appropriate for streaking the ionization dynamics: the contributions from two adjacent laser half cycles are well separated in the momentum distributions and furthermore, the outgoing electron spends little time in the vicinity of the ion so that the Coulomb effects on the trajectory are small. In contrast, with linearly polarized laser pulses, the momentum distributions are peaked at zero momentum, sometimes with a small dip at zero [16, 17]. In this case, the contributions from adjacent half cycles (both centred at zero momentum) overlap each other [18] and the electrons spend more time close to the ion, resulting in larger Coulomb effects and rescattering.

In a simulation, we can eliminate the problems associated with linear streaking by employing a half-cycle pulse. Ionization by such an artificial half-cycle pulse gives rise to a smooth momentum distribution without above-threshold ionization peaks. Furthermore, the distribution is centred at a nonzero momentum because the final vector potential is nonzero or, in other words, because the laser field never changes sign so there is no slowing-down of the ejected electrons by the laser field.

In this work, the streaking by half-cycle pulses is used to gain insight into the ionization dynamics of linearly polarized laser fields. We compare momentum distributions from the time-dependent Schrödinger equation (TDSE) to the predictions of classical models for the continuum dynamics of the electron. In these models we take the Stark shift of the ground state due to the applied laser field into account. The importance of Stark shifts has recently been seen in strong-field ionization and high-order harmonic generation with polar molecules [19, 20].

It turns out that the TDSE results, in particular for high intensity, cannot be fully explained by classical trajectories starting with zero initial velocity at the peak of the field, when Coulomb corrections and the Stark shift are fully taken into account. Our results suggest that ionization occurs preferentially before the peak of the field or else that the employed Coulomb-correction method breaks down at high intensity.

Atomic units are used throughout this article.

2. Theory

The split-operator method [21] is used to solve the TDSE $i\partial_t\Psi(x,t) = \hat{H}(t)\Psi(x,t)$ numerically for a one-dimensional model atom [22] described by the Hamiltonian

$$\hat{H}(t) = -\frac{1}{2}\frac{\partial^2}{\partial x^2} + V(x) + xE(t) \tag{1}$$

with the electron coordinate x, the soft-core potential $V(x) = -1/\sqrt{1+x^2}$ and the laser electric field $E(t)$. In the half-cycle streaking calculations, the field has the form

$$E(t) = \begin{cases} E_0\,\sin(\omega t), & 0 < t < \frac{\pi}{\omega} \\ 0, & \text{else,} \end{cases} \tag{2}$$

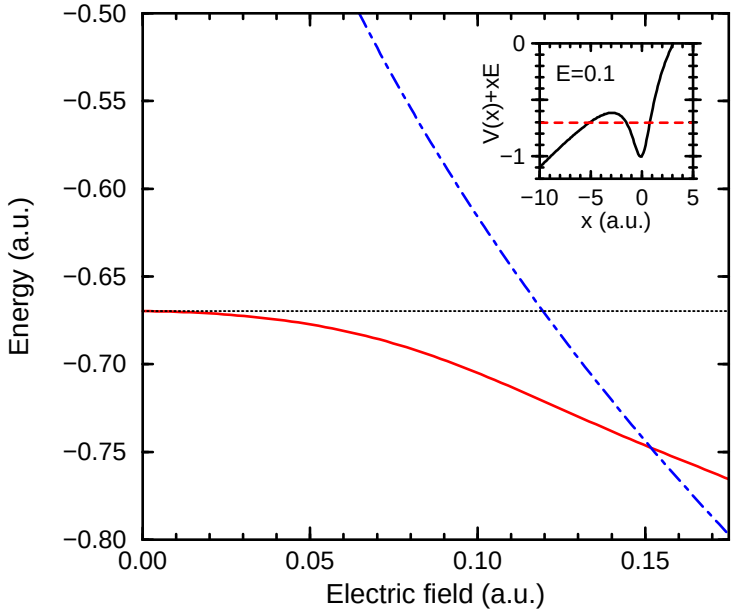

Figure 1. Solid line, ground-state energy of the model atom in the presence of a static electric field. Dotted line, field-free ground-state energy. Dot-dashed line, potential energy at the top of the barrier. The inset shows the potential (solid curve) of the model atom in the presence of an external field E=0.1 together with the corresponding Stark-shifted ground-state energy (dashed line).

where we use various field amplitudes E_0 and a frequency ω corresponding to 800 nm laser wavelength. In the results section, we label the laser pulses by the intensity, which we relate to the field amplitude in the same way as for normal linearly polarized laser pulses. The positive electric field will eject electron density in negative x-direction. The wave function is therefore represented on an "asymmetric" grid ranging from -5570 a.u. to +983 a.u. with equidistant spacing 0.2 a.u. The initial state is the ground state as obtained by imaginary-time propagation [23]. The total duration of real-time propagation is chosen such that the outgoing electron wave packet ends up far away (at least 1000 a.u.) from the ion. Depending on the field strength, propagation durations between 17 and 41 fs have been used. The ionizing part of the wave function is then well separated from the bound part and can be Fourier transformed to obtain the photoelectron momentum distribution. Since the distance from the origin is huge, the error in the momentum distribution due to Coulomb distortion is negligible; namely the energy error is less than 10^{-3} a.u.

To build an accurate streaking model, it is useful to calculate the instantaneous Stark shift of the atomic ground state when subject to the external electric field. This is achieved by propagating the wave function under a constant electric field $E(t) = E_0$ for 108 fs on a symmetric grid ranging from -819 a.u. to +819 a.u. with spacing 0.1 a.u. A Lorentz profile is fitted to the power spectrum of the time-dependent autocorrelation function $C(t) = \langle\Psi(0)|\Psi(t)\rangle$ [21] in order to obtain the energy and the lifetime of the field-dressed state. Figure 1 shows the resulting energy values versus field strength. Also plotted is the potential energy at the top of the barrier formed as the potential is bent by the laser field. We infer from the figure that the barrier-suppression field strength, i.e. the critical field above which the electron can escape over the barrier without tunnelling, is $E_{\rm BS} = 0.15$ a.u. This corresponds to the intensity 0.8 PW/cm^2 for a linearly polarized laser field. Without the Stark shift, the barrier suppression would occur already at the lower field 0.12 a.u. Incidentally, the three-dimensional hydrogen atom has practically the same barrier-suppression field $E_{\rm BS} = 0.15$ a.u., compared to 0.11 a.u. without Stark shift [24].

In order to interpret the momentum spectra in terms of ionization times and trajectories, a classical model is required. We assume that ionization at time t_0 results in an electron appearing

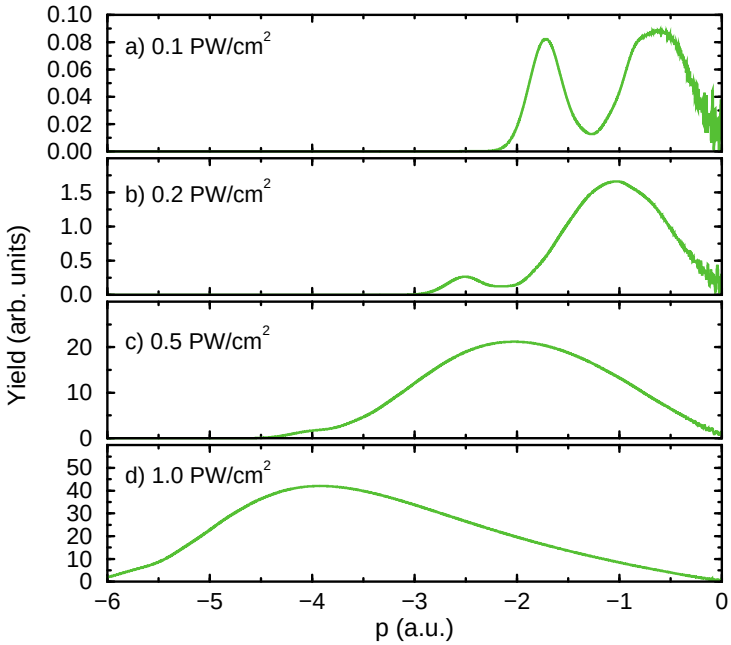

Figure 2. Momentum distributions of outgoing electrons for various intensities as indicated, obtained from the TDSE.

with zero velocity at the exit of the tunnel, i.e. at the (outer) position x_0 satisfying

$$V(x_0) + x_0 E(t_0) = -I_\mathrm{p}, \tag{3}$$

where I_p is the ionization potential. Newton's equation of motion for the electron coordinate is then solved numerically from t_0 until the end of the propagation time using a Verlet algorithm. The force F on the electron includes both the force due to the parent ion as well as the force due to the laser field,

$$F(x,t) = -\partial_x V(x) - E(t). \tag{4}$$

Depending on whether we choose $-I_\mathrm{p}$ to be the field-free ground-state energy or the field-dressed value (see Figure 1), we obtain two different models, denominated in the following as Coulomb-corrected (CC) model and Coulomb-Stark corrected (CSC) model. We also consider the simple man's (SM) model which neglects the force of the ion on the outgoing electron and predicts momenta independent of I_p. For electrons emerging at the peak of the half-cycle pulse, the SM model predicts the final momentum $p_\mathrm{SM} = E_0/\omega$. In this article, we refer to these models as classical models, since the time evolution itself includes no quantum mechanical elements. (Here, quantum mechanics is only needed to find the field-free or field-dressed ground-state energy for the initial position x_0.)

3. Results

Figure 2 shows the final electron momentum distribution after action of a half-cycle pulse for various laser intensities, obtained from the TDSE. We find smooth distributions moving to higher absolute momenta with increasing intensity. For intensities above $0.2\,\mathrm{PW/cm^2}$, the distribution is essentially a simple broad hump which peaks at a momentum value in loose agreement with the simple man's model. For low intensities, we note the presence of a secondary peak at higher absolute momenta. These electrons cannot be explained in terms of the usual tunnelling

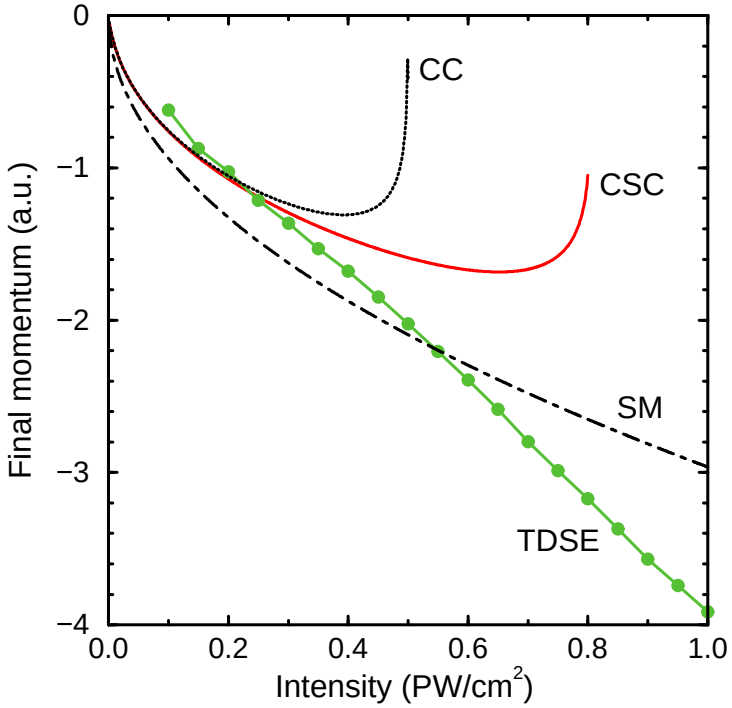

Figure 3. The connected points show the momentum at which the TDSE momentum distribution (see Figure 2) peaks, plotted versus intensity. The other curves are the predictions by the CSC model (solid curve), CC model (dotted curve) and SM model (dot-dashed curve), assuming ionization at the field maximum.

ionization process. Presumably, they are produced by a switch-on effect. Since these unwanted contributions dominate the spectra for intensities below $0.1\,\mathrm{PW/cm^2}$, we restrict ourselves to intensities of $0.1\,\mathrm{PW/cm^2}$ and higher.

Based on the expectation that the peak of the momentum distribution corresponds to ionization at the maximum electric field, we proceed to plot the momentum at the peak position as a function of the intensity, see Figure 3. We compare with the three different classical models, starting the trajectories always at the time of maximum field ($t_\mathrm{m} = 27.6\,\mathrm{a.u.}$). In the CC and CSC models, the trajectories start at the tunnel exit x_0, which is not defined in the over-barrier regime. Therefore, these curves end at the respective barrier-suppression intensities of 0.5 and $0.8\,\mathrm{PW/cm^2}$. Only modest agreement with the numerical results is found. From 0.15 to $0.3\,\mathrm{PW/cm^2}$, the CC and CSC models are in good agreement with TDSE, but at high intensities large discrepancies are seen. Surprisingly, the TDSE predicts momenta that are almost linearly proportional to the intensity, while the SM momenta are exactly proportional to the square root of the intensity. Since there is no explanation for a linear dependence at present, it must be regarded accidental.

Remarkably, high intensities produce electrons that are significantly faster than predicted by the SM model. For an electron with zero initial velocity, this implies having started before the field maximum. Alternatively, the finding could be explained by nonzero initial velocities. In fact, phase-space distributions of tunnel ionization in a static field indicate that the outgoing electrons possess substantial momentum already at the exit of the tunnel [25, 26]. However, it was also noted that the phase-space distributions far away from the barrier do agree with classical trajectories starting with zero velocity at the tunnel exit. This led to the conclusion that zero initial velocity is still the best choice, see [26] for a detailed discussion. Apparently, the situation is different in the over-barrier regime. Since there is no tunnel exit position, one may think of alternative models using nonzero initial velocities. Nevertheless, the predictions of such a model should meet those of the CSC model at the barrier-suppression intensity and we are left

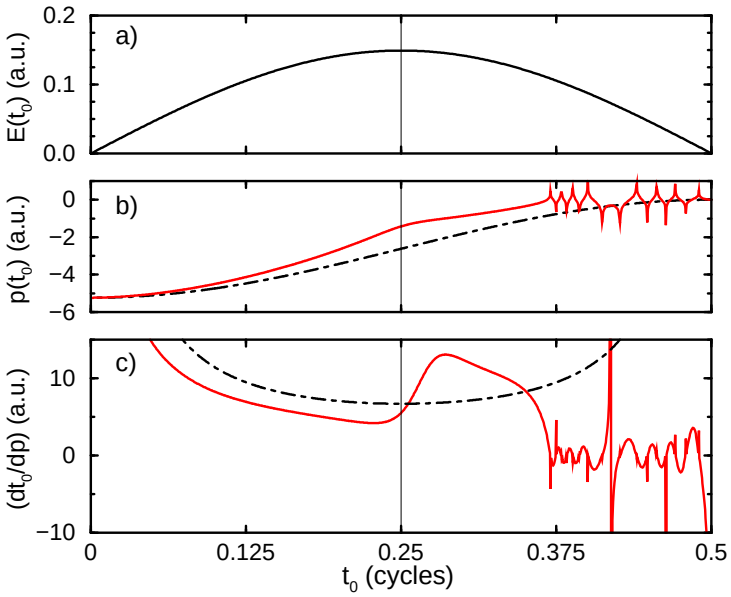

Figure 4. Results of classical models for the intensity $0.78\,\mathrm{PW/cm^2}$. a) Electric field versus ionization time. b) Final momentum p versus ionization time t_0 for the CSC model (solid curve) and the SM model (dot-dashed curve). c) Differential quotient dt_0/dp for the CSC model (solid curve) and the SM model (dot-dashed curve).

with the question how to explain the discrepancies in Figure 3 at intermediate intensities (0.4 to $0.8\,\mathrm{PW/cm^2}$).

For high intensities, depletion of the bound state tends to shift the observed ionization to earlier times since the state may already be substantially depleted at later times. We will see below that depletion alone cannot explain our results. However, we first introduce another important point that has not been taken into account up to now. Momentum distributions show the yield per momentum interval dp, while the notion of maximum ionization at the peak of the field refers to the ionization yield per time interval dt_0. When going from the temporal distribution to a momentum distribution, a factor dt_0/dp should be taken into account, which can affect the position of the maximum. Therefore, the mapping of ionization time t_0 onto final momentum p needs to be investigated in more detail. In the vicinity of the barrier-suppression intensity, $p(t_0)$ is an interesting function as can be seen in Figure 4b, where the results from the SM model and the CSC model are plotted for the intensity $0.78\,\mathrm{PW/cm^2}$, i.e. just below the barrier-suppression intensity. The rapidly oscillating CSC curves for times later than 3/8 cycles reflect the fact that these electrons cannot escape from the binding potential: the acceleration by the laser field is to little to overcome the Coulombic tail of the potential. More importantly, $p(t_0)$ exhibits a shoulder at the time when the field is maximum. The differential quotient dt_0/dp is shown in Figure 4c. This is the factor that has to be multiplied to a temporal distribution in order to obtain a momentum distribution. Apparently this factor, as obtained from the CSC model, gives more weight to ionization after the field maximum than to ionization before the field maximum. Unfortunately, this appears to contradict the TDSE results. On the other hand, we note that the minimum of the curve is very close to the time of the field maximum, suggesting a suppression of these contributions relative to the earlier ones.

Next, we set up a semiclassical model for the calculation of momentum distributions, taking the additional factor dt_0/dp into account. We use the CSC model to map from time to momentum and name the resulting model the CSC-D model. The yield per momentum interval dp is obtained as

$$\frac{dN}{dp} = \frac{dN}{dt_0}\,\frac{dt_0}{dp}, \tag{5}$$

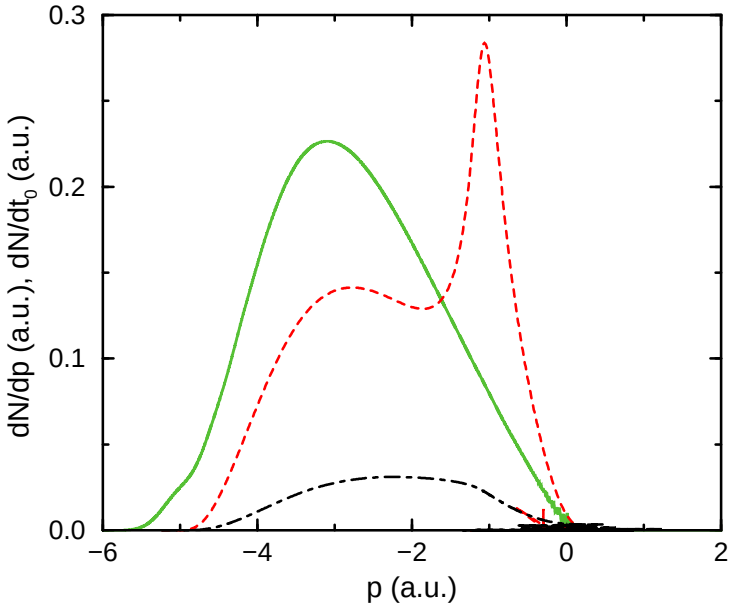

Figure 5. Momentum distributions for intensity 0.78 PW/cm^2 obtained from the TDSE (solid curve), the CSC-D model, Eq. (5) (dashed curve with peak at $p = -1$ a.u.) and the model without the factor dt_0/dp, i.e. the quantity given by Eq. (6) (dot-dashed curve). All data is plotted in atomic units without additional scaling.

where the yield per ionization time interval dt_0 is calculated as

$$\frac{dN}{dt_0} = P(t_0)\,\Gamma(E(t_0)). \tag{6}$$

Here, $P(t_0)$ is the bound population, estimated from the TDSE wave function Ψ by integrating $|\Psi(x, t_0)|^2$ over the region $[-|x_t|, |x_t|]$ with x_t being the position of the barrier maximum at the peak of the field. $\Gamma(E)$ is the decay rate for the model atom subject to the static field E as obtained from the power spectrum of the autocorrelation function (see above). The result of the model for the intensity 0.78 PW/cm^2 is shown as the dashed curve in Figure 5 in comparison with the exact momentum distribution from the TDSE (solid curve). Note that both curves are plotted in the same units, so not only the shape but also the overall height can be compared. The striking result is that the CSC-D model has a broad shoulder at large absolute momenta, peaking at $p = -2.77$ a.u., which is in acceptable agreement with the TDSE result, peaking at -3.1 a.u. In addition, the model predicts a strong peak at around $p = -1$ a.u., which is completely absent from the TDSE distribution. This feature comes from the peak in the factor dt_0/dp at times after the field maximum, see Figure 4c. Leaving out this factor eliminates the spurious peak (see dot-dashed curve in Figure 5), but destroys also the agreement with the TDSE distribution for the faster electrons. (Note, however, that the overall height should not be compared with the other curves because the units are different.) This distribution peaks at -2.24 a.u. as compared to the CSC value -1.42 a.u. for ionization at the field maximum, see Figure 3. Physically speaking, this shift is caused by inclusion of depletion in the model, indicating that depletion alone does not explain the much larger TDSE value of -3.1 a.u.

Why does the CSC-D low-energy peak not appear in the TDSE momentum distribution? The answer to this question seems to lie beyond our (semi)classical ionization models. The fact that a wide range of ionization times after the peak of the field contributes to a narrow range of momenta (see Figure 4b) may enable interferences between the different ionization times. A more advanced semiclassical model could assign an initial momentum uncertainty for each ionization time and assign phases to the different trajectories. Desctructive interference between different pathways to the same final momentum could lead to suppression in certain momentum

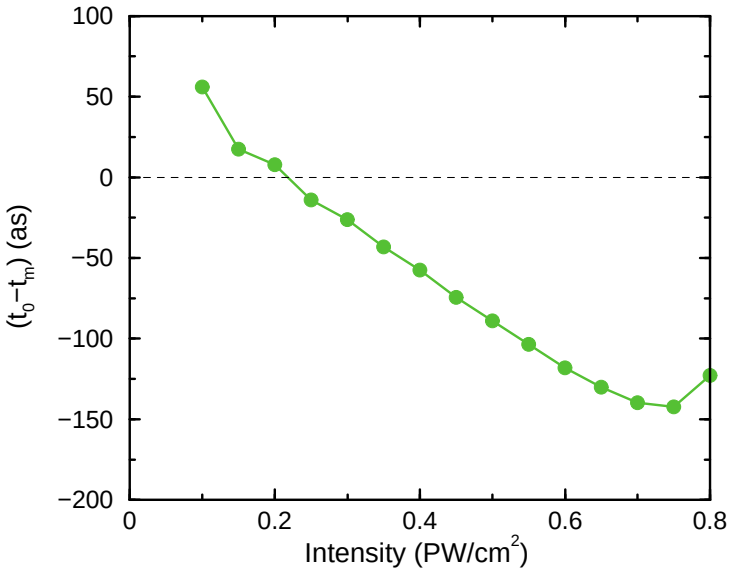

Figure 6. Ionization times versus intensity obtained from the TDSE momentum distributions converted to temporal distributions using the CSC model. Plotted is the time shift relative to the maximum of the electric field.

ranges.

Finally – in the spirit of streaking – we calculate the ionization times from the momentum distributions. This is done by converting the momentum distributions to temporal distributions by multiplication with dp/dt_0 as obtained from the CSC model. In the temporal distribution, we search for the position t_0 of the peak and interpret it as the time of most probable ionization. Since we have not implemented a classical model for the over-barrier regime at present, we carry out this analysis only up to the barrier-suppression intensity $0.8\,\mathrm{PW/cm^2}$. Figure 6 shows the obtained deviation of the ionization time t_0 from the time t_m of maximum electric field in attoseconds. For the lowest intensities, ionization takes place with highest probability slightly after the field maximum, while for higher intensities ionization occurs preferentially before the field maximum. These time shifts are small compared to the optical cycle but large compared to the tunnelling delay time found in the angular streaking experiments. Note that the result shown in Figure 6 is not corrected for the depletion effect. One could carry out such a correction by using Eq. (6) together with numerically obtained values for $P(t_0)$. The resulting values, however, are rather sensitive to the choice of the integration limits when integrating $|\Psi|^2$ over space. Roughly, the correction is found to be less than 50 attoseconds at the high intensities, i.e. the most probable ionization still occurs before the field maximum.

4. Conclusion

Streaking by a half-cycle laser pulse is a useful theoretical tool for the time-resolved study of strong-field ionization. For moderate laser intensities, the peak position in the electron momentum distribution agrees with the predictions of the Coulomb-corrected classical models, indicating that ionization occurs almost instantaneously at the time when the electric field reaches its maximum. At high intensities, the peak position deviates from the classical models based on ionization at the field maximum. The results suggest that ionization occurs preferentially at earlier times or that the employed Coulomb-correction method breaks down at high intensity. Depletion alone is not sufficient to cause the effect. Furthermore, the observed suppression of ionization later than the field maximum cannot be explained by the (semi)classical models that we have used. It appears that a more advanced semiclassical theory, allowing for interference of different

trajectories, is needed. One such theory could be a Coulomb-corrected strong-field approximation beyond the saddle-point approximation. The application of the strong-field approximation to half-cycle streaking may be the subject of future work.

We have argued that the conversion from momentum to temporal distributions should take the nonconstant factor dp/dt_0 into account. In angular streaking, a similar effect may play a role in the conversion from angle θ to ionization time . However, the effect is probably less important than in the linear streaking, since for example a perfectly circularly polarized laser field leads to $d\theta/dt_0$ =const if depletion is negligible.

Acknowledgements

The author thanks his group members, in particular J. Henkel, E. van der Zwan and I. Dreißigacker, for the critical reading of the manuscript. Discussions with Lars B. Madsen have been very useful. The funding of the Centre for Quantum Engineering and Space-Time Research (QUEST) by the Deutsche Forschungsgemeinschaft is gratefully acknowledged.

References

[1] E. Goulielmakis, M. Schultze, M. Hofstetter, V.S. Yakovlev, J. Gagnon, M. Uiberacker, A.L. Aquila, E.M. Gullikson, D.T. Attwood, R. Kienberger, F. Krausz and U. Kleineberg, Science **320** 1614 (2008).
[2] H. Niikura, F. Légaré , R. Hasbani, A.D. Bandrauk, M. Yu. Ivanov, D.M. Villeneuve and P.B. Corkum, Nature **417** 917 (2002).
[3] S. Baker, J. Robinson, C.A. Haworth, H. Teng, R.A. Smith, C.C. Chirilă, M. Lein, J.W.G. Tisch and J.P. Marangos, Science **312** 424 (2006).
[4] S. Haessler, J. Caillat, W. Boutu, C. Giovanetti-Teixeira, T. Ruchon, T. Auguste, Z. Diveki, P. Breger, A. Maquet, B. Carré, R. Taïeb and P. Salières, Nature Phys. **6** 200 (2010).
[5] M. Meckel, D. Comtois, D. Zeidler, A. Staudte, D. Pavičić, H.C. Bandulet, H. Pépin, J.C. Kieffer, R. Dörner, D.M. Villeneuve and P.B. Corkum, Science **320** 1478 (2008).
[6] G.L. Yudin and M. Yu. Ivanov, Phys. Rev. A **64** 013409 (2001).
[7] O. Smirnova, Y. Mairesse, S. Patchkovskii, N. Dudovich, D.M. Villeneuve, P.B. Corkum and M. Yu. Ivanov, Nature **460** 972 (2009).
[8] C.D. Lin, A.-T. Le, Z. Chen, T. Morishita and R. Lucchese, J. Phys. B **43** 122001 (2010).
[9] P.B. Corkum, Phys. Rev. Lett. **71** 1994 (1993).
[10] G.G. Paulus, W. Becker, W. Nicklich and H. Walther H, J. Phys. B **27** L703 (1994).
[11] Y. Mairesse, A. de Bohan, L.J. Frasinski, H. Merdji, L.C. Dinu, P. Monchicourt, P. Breger, M. Kovačev, R. Taïeb, B. Carré, H.G. Muller, P. Agostini and P. Salières, Science **302** 1540 (2003).
[12] P. Eckle, M. Smolarski, P. Schlup, J. Biegert, A. Staudte, M. Schöffler, H.G. Muller, R. Dörner and U. Keller, Nature Phys. **4** 565 (2008).
[13] P. Eckle, A.N. Pfeiffer, C. Cirelli, A. Staudte, R. Dörner, H.G. Muller, M. Büttiker and U. Keller, Science **322** 1525 (2008).
[14] L.V. Keldysh, Sov. Phys. JETP **20** 1307 (1965).
[15] M. Büttiker and R. Landauer, Phys. Rev. Lett. **49** 1739 (1982).
[16] A. Rudenko, K. Zrost, C.D. Schröter, V.L.B. de Jesus, B. Feuerstein, R. Moshammer and J. Ullrich, J. Phys. B **37** L407 (2004).
[17] A. Rudenko, K. Zrost, T. Ergler, A.B. Voitkiv, B. Najjari, V.L.B. de Jesus, B. Feuerstein, C.D. Schröter, R. Moshammer and J Ullrich, J. Phys. B **38** L191 (2005).
[18] F. Lindner, M.G. Schätzel, H. Walther, A. Baltuška, E. Goulielmakis, F. Krausz, D.B. Milošević, D. Bauer, W. Becker and G.G. Paulus, Phys. Rev. Lett. **95** 040401 (2005).
[19] L. Holmegaard, J.L. Hansen, L. Kalhøj, S.L. Kragh, H. Stapelfeldt, F. Filsinger, J. Küpper, G. Meijer, D. Dimitrovski, M. Abu-samha, C.P.J. Martiny and L.B. Madsen, Nature Phys. **6** 428 (2010).
[20] A. Etches and L.B. Madsen, J. Phys. B **43** 155602 (2010).
[21] M.D. Feit, J.A. Fleck, Jr., and A. Steiger, J. Comput. Phys. **47** 412 (1982).
[22] J. Javanainen, J.H. Eberly and Q. Su, Phys. Rev. A **38** 3430 (1988).
[23] R. Kosloff and H. Tal-Ezer, Chem. Phys. Lett. **127** 223 (1986).
[24] R. Shakeshaft, R.M. Potvliege, M. Dörr, and W.E. Cooke, Phys. Rev. A **42** 1656 (1990).
[25] A. Czirjak, R. Kopold, W. Becker, M. Kleber and W.F. Schleich, Optics Commun. **179** 29 (2000).
[26] M. Yu. Ivanov, M. Spanner and O. Smirnova, J. Mod. Opt. **52** 165 (2005).